



In-flight enhancement of the optical frequency accuracy of an integral-path differential absorption lidar thanks to a rugged, airborne self-referenced frequency comb

MATHIEU QUATREVALET,^{1,*} MARTIN WOLFERSTETTER,² BENJAMIN SPRENGER,² MARC FISCHER,² RONALD HOLZWARTH,² AND ANDREAS FIX¹ 

¹Deutsches Zentrum für Luft- und Raumfahrt, Institut für Physik der Atmosphäre, Oberpfaffenhofen, Germany

²Menlo Systems GmbH, 82152 Martinsried, Germany

*Mathieu.Quatrevalet@dlr.de

Abstract: Airborne and spaceborne integral-path differential absorption (IPDA) lidar has the potential to deliver column measurements of the major greenhouse gases influenced by human activity with the high accuracy that is required to significantly reduce the uncertainties in our estimations of surface fluxes of methane and carbon dioxide by inverse modelling. A prerequisite is the highly accurate knowledge of the emitted wavelengths, especially for carbon dioxide in the 1.6- μm region, where a long-term optical frequency knowledge accuracy of the online channel down to a few tens of kHz is required. Deutsches Zentrum für Luft- und Raumfahrt's airborne IPDA lidar for simultaneous measurements of carbon dioxide at 1.57 μm and methane at 1.64 μm , CHARM-F, uses a specifically developed frequency reference unit based on optimized wavelength modulation spectroscopy which can reach the required accuracy in a stabilized laboratory environment, but whose in-flight performance in the more challenging aircraft environment could not be independently validated. In the frame of the Carbon Dioxide and Methane Mission (CoMet) field campaigns in 2018 and 2022, CoMet 1.0 and CoMet 2.0 Arctic, respectively, a cooperation with Menlo Systems GmbH made it possible to bring a prototype of a new generation of portable and rugged self-referenced frequency combs (SRFCs) on board the German research aircraft HALO. This airborne frequency comb served as an independent frequency reference to characterize the performance of the carbon dioxide channel of CHARM-F's frequency reference system in flight. We report here on the frequency stability measurements carried out during the CoMet 2.0 Arctic campaign and demonstrate the potential of such portable SRFCs as next-generation frequency references for atmospheric lidars.

Published by Optica Publishing Group under the terms of the [Creative Commons Attribution 4.0 License](https://creativecommons.org/licenses/by/4.0/). Further distribution of this work must maintain attribution to the author(s) and the published article's title, journal citation, and DOI.

1. Introduction

An Integral-Path Differential Absorption (IPDA) lidar for atmospheric trace gases uses its own, spectrally narrow laser light source to sound the atmosphere at two or more wavelengths in the vicinity of a single absorption line or feature of the trace gas. In contrast to passive remote sensing which relies on solar light, it has the ability to measure at night, at all latitudes and all seasons. Furthermore, by positioning the so-called online wavelength in the wing of the pressure broadened absorption line, the vertical sensitivity of the measurement can be tailored to target the lowermost atmospheric layers, where the concentration gradients due to surface fluxes are strongest [1,2]. However, this puts a stringent requirement on the knowledge of the absolute online wavelength,

because of the steep slope of the absorption cross-section in the wing. For CO₂ in the 1.6-micron region, this translates to a knowledge requirement of the order of a few tens of kHz [1,2], a level typically requiring advanced spectroscopic techniques such as Doppler-free spectroscopy and suitable, strong absorption lines. Nevertheless, in the case of Deutsches Zentrum für Luft- und Raumfahrt's (DLR's) airborne IPDA lidar for simultaneous measurements of carbon dioxide and methane, CHARM-F (CO₂ and CH₄ Atmospheric Remote Monitor – Flugzeug), a frequency reference subsystem was developed that uses classical Wavelength Modulation Spectroscopy (WMS) applied to the same Doppler-broadened CO₂ line in an absorption cell as the one used for the atmospheric IPDA measurement. Careful optimization of the WMS scheme with the help of one of the first commercially-available stationary Self-Referenced Frequency Comb (SRFC), a FC1500 from Menlo Systems GmbH, made it possible to achieve the specification in a controlled laboratory environment, but its performance in the more challenging aircraft environment remained largely uncharacterized so far.

In 2015, an opportunity arose for a cooperation between DLR and Menlo Systems, who had started working on the development of a new generation of compact and rugged SRFCs, now commercialized under the trademark “SmartComb”, and get access to a prototype as demonstrator of a next-generation frequency reference for lidar spectroscopy. The prototype, dubbed FOKAL (Faser-Optischer Kammgenerator für Angewandte Lidar Spektroskopie), was subsequently certified to fly on HALO alongside CHARM-F and monitor FRERES's online wavelength, and became the first airborne SRFC in the frame of the CoMet 1.0 field campaign in May-June 2018 [3,4], while a second deployment took place in the frame of the CoMet 2.0 Arctic campaign in Canada in August-September 2022. For this campaign, FRERES was improved and worked rather flawlessly, so that in the following this data was used to characterize its in-flight performance.

2. Menlo Systems' portable and rugged SRFC, “FOKAL”

2.1. SRFCs as independent, absolute optical frequency references

A self-referenced frequency comb is essentially the combination of an optical frequency comb, i.e. a mode-locked, pulsed femtosecond laser producing a comb-like spectrum with evenly spaced modes, and the subsequent detection and stabilization of the comb's two free parameters, the repetition rate (RR), f_{rep} , and the Carrier-Envelope Offset (CEO) frequency, f_{CEO} , which corresponds to the offset of the comb with respect to frequency zero. The optical frequency ν_n of mode number n can be written as:

$$\nu_n = f_{CEO} + n f_{rep} \quad (1)$$

For detection of the CEO frequency a supercontinuum-generating optical fiber that broadens the comb to an octave-spanning spectrum via strong optical non-linearities is used [5,6]. The octave-spanning spectrum and second harmonic generation make it possible to produce a beat note between comb mode number $2n$ on the shorter wavelength side of the spectrum and the frequency doubled mode number n on the longer wavelength side of the spectrum by means of an f-to-2f interferometer, cancelling out the second term on the right-hand-side of Eq. (1) and giving access to the value of f_{CEO} , hence the “self-referenced” denomination. Since f_{rep} and f_{CEO} are both in the Radio Frequency (RF) domain, this opens up the possibility of stabilizing the comb modes against a wealth of readily available highly accurate RF oscillators whose stability is thus transferred into the optical domain.

SRFCs lend themselves as independent frequency references for the determination of the absolute optical frequency and long-term stability of cw lasers as long as sufficient spectral power is present in the comb spectrum around the cw laser wavelength, so that a beat frequency f_{cw} between the nearest comb mode and the cw laser can be detected. For this purpose, a so-called “Beat Detection Unit” (BDU) is typically used to combine the light from both lasers and send it

through a specific, narrow optical bandpass filter to improve the SNR of the beat signal. The determination requires a first independent estimate $\tilde{\nu}_{CW}$ of the cw laser's optical frequency with an accuracy better than half of f_{rep} , in order to infer the comb mode number. If the sign of f_{cw} is not known, this is done by calculating n_+ and n_- , the fractional comb mode numbers for positive f_{cw} and negative f_{cw} :

$$\begin{aligned} n_+ &= \frac{\tilde{\nu}_{CW} - f_{cw} \pm f_{CEO}}{f_{rep}} \\ n_- &= \frac{\tilde{\nu}_{CW} + f_{cw} \pm f_{CEO}}{f_{rep}} \end{aligned} \quad (2)$$

and by selecting the fractional comb mode number that is closest to the nearest integer. The absolute optical frequency of the CW laser ν_{CW} is then simply given by:

$$\nu_{CW} = \pm f_{CEO} \pm f_{beat} + \text{round}(n_{\pm}) \times f_{rep} \quad (3)$$

where all signs are now known.

The first estimate $\tilde{\nu}_{CW}$ is typically provided by an independent, coarse measurement such as a wavemeter, or by the observation of narrow absorption lines in a gas cell.

2.2. Menlo Systems' portable and rugged SRFC, "FOKAL"

Femtosecond lasers are normally sensitive to vibrations, pressure, temperature and humidity variations, however, using polarization maintaining fibers the laser can be sufficiently decoupled from these perturbations. Menlo Systems GmbH further developed a proprietary technology, dubbed "Fig. 9", based on the so-called nonlinear amplified loop mirror technique [7,8]. As a testimony to its potential robustness, this technology has been successfully tested and operated on sounding rocket flights during the microgravity missions TEXUS 51 and 53 [9]. FOKAL, housed in a single 19"-rack, 3U package, is also based on the "Fig. 9"-technology and, to a large extent, was a prototype of Menlo's current "SmartComb" product line of portable and rugged SRFCs. It is important to note that it was not specifically designed to specifications relevant for airborne operation, but rather as a laboratory device.

FOKAL is fully fiber-based and its femtosecond oscillator has a repetition rate of 100 MHz. A simplified block diagram of the device is displayed in Fig. 1, also showing its optical interface with FRERES.

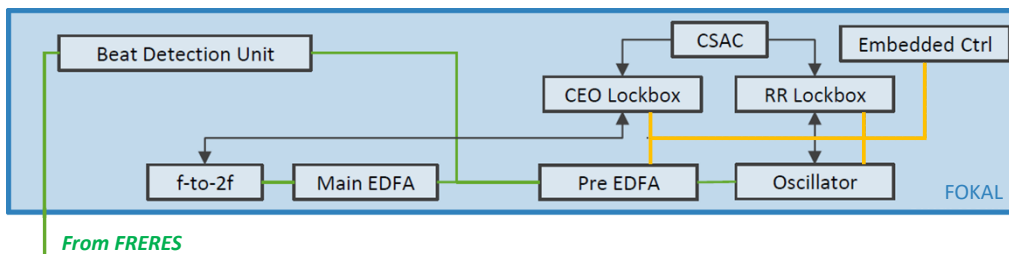


Fig. 1. Simplified block diagram of FOKAL. Green: polarization-maintaining, single-mode optical fibers. Black: analog interfaces. Orange: digital interfaces. EDFA: Erbium-Doped Fiber Amplifier. CEO: Carrier-Envelope Offset. RR: Repetition Rate. CSAC: Chip-Scale Atomic Clock. See text for details.

So-called "lockboxes" for the CEO and RR locks, orchestrated by an embedded controller, are meant to provide fully automated beat detection and comb locking, using a combination of slow and fast actuators within the oscillator and the fiber amplifiers. The embedded controller is also equipped with an Ethernet interface (not shown in Fig. 1) that was connected to a data logging

laptop used by the CHARM-F operators to store the FOKAL data at a rate of 1 Hz during the flights.

While access to the signal from the GPS antenna can be provided on board HALO and a GPS-disciplined, Oven-Controlled Quartz Oscillator (OCXO) could theoretically have been used as RF reference for FOKAL and would have enabled long-term stabilities orders of magnitude better than the most stringent IPDA online wavelength knowledge accuracy requirement (see also section 2.3), this would have complicated the integration and certification process on HALO as such a device would have had to be integrated outside of the mechanical envelope of FOKAL, leading to additional flight certification costs and delays. Instead, and as illustrated in Fig. 1, it was decided to use a Chip-Scale Atomic Clock (CSAC) from Symmetricom (now Microchip), model SA.45s-02, that was readily available at Menlo Systems GmbH for integration. The latter reaches an Allan deviation below 7×10^{-12} after 1000 s averaging [10], still orders of magnitude better than the requirement.

2.3. Pre- and post-campaign calibration using stationary, GPS-referenced SRFC

Part of the laboratory infrastructure at DLR is a stationary SRFC, model FC1500 also from Menlo Systems GmbH. This device has a repetition rate/free spectral range of 250 MHz and is equipped with optical amplifiers and BDUs optimized for the operating wavelengths of CHARM-F and referenced to a GPS-disciplined OCXO (K + K GPS6). The latter reaches a relative long-term stability of 3×10^{-12} , which translates into an optical frequency stability of the SRFC modes of better than 0.6 kHz in the 180-190 THz region - a good approximation of an ideal absolute frequency reference for our purposes. In combination with a wavemeter with an accuracy better than 100 MHz (HighFinesse WS6/100) for the determination of the comb mode number, the system makes it possible to measure the absolute frequency of any external cw laser and its variations down to order of magnitudes better than the most stringent IPDA online wavelength knowledge accuracy requirement.

In order to absolutely calibrate FOKAL referenced to its CSAC using the stationary FC1500, the online seed laser was used as a probe, in that it was phase-locked to the FC1500 and two FOKAL measurements were performed: one with the FC1500 referenced to its GPS-disciplined oscillator, and one with the FC1500 referenced to FOKAL's CSAC. The offset between the measured beat frequencies gives direct access to the optical frequency offset of FOKAL with respect to the FC1500. Furthermore, the measurement was repeated at the end of October 2022, in order to have some information on the long-term drift of the CSAC-referenced SRFC over the campaign. The results of both calibrations are summarized in Table 1.

Table 1. Results of the absolute calibration of FOKAL before (May 2022) and after (October 2022) the CoMet 2.0 Arctic campaign

Date	Absolute optical frequency offset of FOKAL
21.06.2022	0.0348 ± 0.0015 MHz
20.10.2022	-0.0105 ± 0.0011 MHz

The absolute drift of FOKAL over the four-months period between the two measurements thus amounts to about 45 kHz or 11 kHz/month, which is in line with the specified CSAC aging, quoted at 3×10^{-10} /month [10] and equivalent to 60 kHz/month at an optical frequency of 190 THz (corresponding to the CO₂ online seeder wavelength's of 1572 nm).

3. FREquency REference Subsystem (FRERES) for DLR's CHARM-F lidar

3.1. Description

The overall architecture of CHARM-F has been outlined in a number of publications [e.g. 11,12]. Its transmitters are based on Optical Parametric Oscillators (OPO) pumped by double-pulse, Diode-Pumped Solid State Nd:YAG lasers and achieve single-frequency operation by means of injection-seeding. Thanks to a solid-state optical switch, the OPO cavity is alternately seeded by two cw lasers for the online and offline wavelength, respectively. The OPO cavity is actively kept in resonance with the online seed laser by means of a piezoelectric element on one of its mirrors, with the error signal generated via a heterodyne technique that was first introduced in DLR's airborne water vapor differential absorption lidar [13,14]. The same heterodyne technique is used in reverse to lock the offline seeder to another OPO cavity mode closest to the specified offline wavelength. Thanks to both of these feedback loops, the long-term stability/knowledge accuracy of the OPO pulses' wavelengths follows the long-term wavelength stability/knowledge accuracy of the seed lasers' wavelengths.

In order to achieve the particularly stringent online wavelength knowledge requirement, a specific FREquency REference Subsystem (FRERES) was developed in-house at DLR. It mostly makes use of telecom-type, Distributed Feed-Back (DFB) laser diodes (NEL model NLK1L5GAAA for the CO₂ channel), except for the CO₂ online seed laser close to 1572 nm, which is a DFB fiber laser (NP Photonics model RLFM-25), selected for its inherently better short-term stability. The frequency referencing scheme is conceptually illustrated in Fig. 2. In addition to the online and offline seed lasers, a third cw laser with optical frequency ν_{REF} , hereafter referred to as the reference laser, generates a derivative error signal $\varepsilon = \varepsilon(\nu_{REF})$ via wavelength modulation spectroscopy (WMS). The WMS is implemented via a software lock-in amplifier (LIA) in Labview and hosted on an embedded computer within a PXI chassis equipped with several National Instruments control/acquisition cards. One analog output produces a sinusoidal modulation signal at a frequency of a few kHz for the current modulation input of the reference laser, part of whose light is sent through a multi-pass absorption cell of the astigmatic Herriott type (Aerodyne Research model AMAC-36) with an optical path length of 36 m and filled with carbon dioxide and methane at partial pressures of about 20 mbar and 6 mbar, respectively. The same Labview program processes the modulated signal recorded with a large-area (5 mm diameter), amplified Germanium photodiode (Thorlabs PDA50B) behind the absorption cell.

Simultaneously, the computer program generates a stream of TTL (Transistor-Transistor Logic) compatible gates synchronized to the extrema of the modulation waveform at a digital output of the acquisition card. These gates trigger measurements with a high-bandwidth frequency counter (Vigo Systems T3200U with frequency range up to 3.5 GHz) connected to a fast near-infrared photodetector (InGaAs, Menlo Systems FDP310) detecting the beat frequency produced between reference and online seed laser behind an optical fiber combiner. The optical frequency offset $\Delta\nu$ of the online seed laser with respect to the reference laser, averaged over the time window between two successive time steps of the lock-in amplifier t_{i-1} and t_i is defined as:

$$\Delta\nu(t_i) = \frac{1}{2} \cdot (\langle f_{up} \rangle_{t_{i-1}}^{t_i} - \langle f_{down} \rangle_{t_{i-1}}^{t_i}) \quad (4)$$

where f_{up} , respectively f_{down} , are the individual beat frequency measurements within gates corresponding to the "positive" (in terms of optical frequency), respectively "negative" extrema of the modulation waveform within the averaging window.

Étalon fringes, produced by light scattering and/or overlapping reflections at the optical surfaces, are a known issue with multi-pass absorption cells which strongly hinders the achievable signal-to-noise ratio in tunable diode laser spectroscopy and the use of Doppler-broadened absorption lines as spectral references. Therefore, a substantial amount of effort was invested

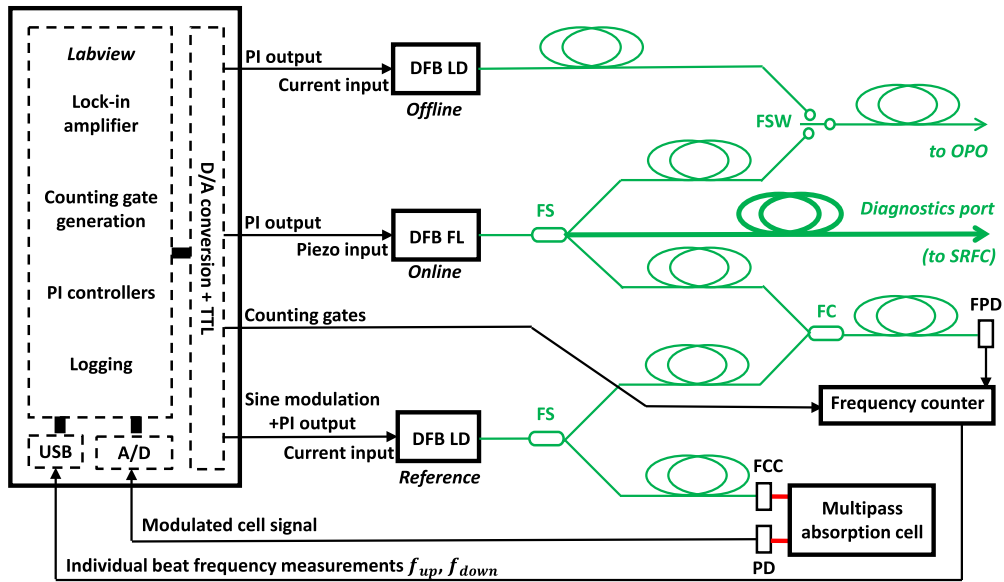


Fig. 2. Simplified architecture of the CO₂ channel of CHARM-F's FRERES subsystem. Green: polarization-maintaining, single-mode optical fibers. Red: free-space laser beam. FS: fiber splitter. FC: fiber combiner. FSW: Fast optical switch. FCC: fiber-coupled collimator. PD: Photodiode. FPD: Fast Photodiode. DFB LD: Distributed Feed-Back Laser Diode. DFB FL: Distributed Feed-Back Fiber Laser. See text for details.

during the development of CHARM-F in implementing various technical measures to reduce the sensitivity of the FRERES setup to these interference fringes:

- (1) The cell itself is designed in such a way as to minimize overlaps on the mirrors and the free spectral range of interference fringes [15,16];
- (2) The use of a large-area photodiode behind the cell prevents any variable spatial trimming of the fringe interference patterns within the collimated beam;
- (3) The modulation amplitude of the reference laser is chosen so that corresponds to an integer number of cycles of the dominating fringe;
- (4) A special reference waveform is implemented in the digital lock-in amplifier to enhance the contrast of the signal from the absorption line relative to that from the fringes, in an analogous manner to [17].

Software-implemented feedback loops, based on Proportional-Integral controllers, act on the bias current of the reference laser and on the piezo voltage of the online seed laser via analog outputs of the acquisition cards in order to keep the former near the CO₂ line center, at the zero-crossing ν_0 defined as $\varepsilon(\nu_0) = 0$, and the latter near the desired frequency offset with respect to the reference laser in the line wing. Since the high-frequency jitter of the outgoing laser pulses is dominated by (mostly mechanical) jitter of the OPO cavity, and since the requirement is on the long-term accuracy of the wavelength knowledge rather than on the actual stability, slow feedback loops (2 Hz processing rate during CoMet 2.0) are sufficient as long as the error signal and frequency offset are logged for later determination of the absolute optical frequency in the IPDA retrieval. For small frequency deviations of the reference lasers away from the zero-crossing, it is

simply calculated through:

$$\nu_{on, FRERES}(t_i) = \nu_0 + \frac{d\nu}{d\varepsilon}(\nu_0)\varepsilon(t_i) + \Delta\nu(t_i) \quad (5)$$

where $d\nu/d\varepsilon(\nu_0)$ is the derivative of optical frequency with respect to ε at the zero-crossing.

As illustrated in Fig. 2, the optical link to the FC1500 or to FOKAL, located in a different rack in the rear part of the aircraft, is provided by a Polarization-Maintaining fiber from an additional splitter branch downstream from FRERES's online seed laser, normally used for diagnostics in the laboratory to the external input of FOKAL's BDU.

3.2. Pre-campaign spectral calibration with the stationary, GPS-referenced SRFC

The stationary SRFC introduced in section 3.3 played a crucial role as an independent absolute spectral reference in the afore-mentioned reduction of the WMS scheme's sensitivity to étalon fringes. In addition, it fulfills the important role of an independent calibration device for the preparation of flight campaigns.

The pre-campaign calibration of FRERES consists in determining the position of the zero-crossing ν_0 and the first derivative of the WMS error signal in its vicinity $d\varepsilon/d\nu(\nu_0)$ as defined in section 3.1. This is achieved by adding a slow, sawtooth component to the reference laser's modulation signal in order to repeatedly scan the $\varepsilon(\nu_{ref})$ curve around the zero-crossing point, on the one hand; and offset-locking the online seed laser to the FC1500 in the vicinity (i.e. much closer to the latter than half of the FC1500's free spectral range of 250 MHz) of the zero-crossing by means of phase-lock loop, on the other hand, in which case the following relationship applies at all times:

$$\nu_{ref} = (\nu_0 - \nu_{on,FC1500}) + \Delta\nu \quad (6)$$

Here, $\nu_{on,FC1500}$ is the known, fixed absolute optical frequency of the comb-locked online seed laser, derived via the comb equation as described in section 2.1, only using the known CO₂ line center position instead of $\nu_{on, FRERES}$ as a first estimate for the comb mode number determination.

A polynomial fit is then applied to each $\varepsilon(\nu_{ref})$ scan, using Eq. (6) to calibrate the x-axis, and the fit coefficients are averaged over many scans to reduce the uncertainty. In preparation for CoMet 2.0 Arctic, this procedure was carried out at the end of May 2022, about two months before the start of the campaign, and yielded the results presented in Table 2.

Table 2. Results of FRERES spectral calibration on 30.05.2022

Parameter	Symbol	Measurement method	Value
Frequency of locked online seed laser	$\nu_{on,FC1500}$	FC1500 SRFC	190705485.967 ± 0.001 MHz
Offset between zero-crossing and frequency of online seed laser	$\nu_0 - \nu_{on,FC1500}$	Polynomial fits to 86 $\varepsilon(\nu_{ref})$ scans	-6.910 ± 0.150 MHz
Optical frequency of reference laser at zero-crossing	ν_0	From previous parameters	190705479.057 ± 0.150 MHz
Derivative at zero-crossing	$d\nu/d\varepsilon(\nu_0)$	Polynomial fits to 86 $\varepsilon(\nu_{ref})$ scans	0.090 ± 0.002 MHz

The values in bold in Table 2 were the ones inserted in Eq. (5) and used throughout the campaign to calculate the absolute online optical frequency. It should be noted that, due to issues with the absorption cell after dismounting CHARM-F from HALO, no post-campaign calibration of FRERES could be carried out.

4. Flight data and data processing

CHARM-F and FOKAL were integrated onto HALO in the course of July 2022, and remained on board during the 19 scientific flights of the CoMet 2.0 campaign that took place between August 4th 2022 and September 16th 2022, including the transfer flights from Oberpfaffenhofen, Germany to Edmonton, Canada, and back. CHARM-F was operated at all times during these flights and the CHARM-F operators on board also strove to keep FOKAL in lock and acquire FOKAL data at all times.

However, with a mix of in-situ and remote sensing instruments in the scientific payload onboard HALO, the CoMet 2.0 Arctic flight planning called for frequent altitude changes, which in turn led to frequent pressure and associated temperature changes in the HALO cabin. These were at times fast enough to overwhelm FOKAL's "slow actuators", leading to occasional loss of the CEO and/or repetition rate lock. This happened mostly during and after the transitions from so-called "remote sensing legs" at cruise altitudes of about 8 km to so-called "in-situ legs" at a low altitude of about 1 to 2 km in the planetary boundary layer. Furthermore, it was often necessary to alter the repetition rate after such events in order to recover the locked state and/or improve the SNR of the beat signal, so that the online seed laser was not always beating with the same comb mode number, and not always on the same side of the comb mode.

FRERES performed nominally throughout all flights, and only one peculiarity must be noted. After the first 7 flights, and for reasons outside of the scope of this paper, the modulation amplitude of the reference (which can be readily monitored from the FRERES data itself as it simply equals $f_{up} + f_{down}$) was changed from 1.11 GHz to 1.67 GHz, which had an influence on the results as it will become evident in section 5.1.

Finally, although both the FRERES computer and the FOKAL data logging laptop were synchronized to the aircraft's onboard network time protocol (NTP) server, we observed a flight-dependent time shift between the FOKAL and FRERES time. This made it necessary to repeat the pre-processing steps for the FOKAL data, listed in Table 3, for a range of time shifts δt applied to the FOKAL data.

Table 3. Data processing steps for the calculation of the $\nu_{on, FOKAL}$ time series for each flight. The steps between thick lines are repeated for a range of time shifts

Step number	Description	Output
1	Filtering of unlocked FOKAL data and data with insufficient margins on the following parameters: SNR of CEO and RR lock, SNR of beat signal with online seed laser, position of beat signal within the bandwidth of the BDU's RF filter	Filtered FOKAL data
2	Interpolation of the 1-Hz FOKAL data to the 2-Hz temporal grid of FRERES for a given time shift δt	Interpolated FOKAL data for δt
3	Determination of the comb mode number and sign of the beat signal from Eq. (5)	Comb mode number and sign of beat signal
4	Calculation of $\nu_{on, FOKAL}$ from Eq. (6)	$\nu_{on, FOKAL}(\delta t)$
5	Removal of the remaining outliers.	$\nu_{on, FOKAL}(\delta t)$ without outliers
6	Determination of the time shift $\delta t_{0, flight}$ between FOKAL and FRERES data that minimizes $\sigma(\nu_{on, FOKAL}(\delta t) - \nu_{ON, FRERES})$	$\delta t_{0, flight}$ and final $\nu_{on, FOKAL}$ time series

Overall, over 60 hours of high-quality FRERES and FOKAL data spanning 13 flights could be acquired during the campaign and successfully pre-processed for this work. An exemplary

time series is depicted in Fig. 3. It was acquired during the return transfer flight from Canada to Germany, which provided almost uninterrupted time series thanks to the stable cabin conditions at constant cruise altitude. The qualitative agreement between both devices is remarkable at all timescales, considering that the two measurements are completely independent from each other and rely on two unrelated physical mechanisms. Both devices capture the same slow drifts of the fiber laser with a magnitude of a few MHz around the setpoint of 500 MHz, and at time constants of a few seconds to a few tens of seconds, before the influence of FRERES's feedback loop (with its processing rate of 2 Hz and corresponding time constant of 5s) sets in.

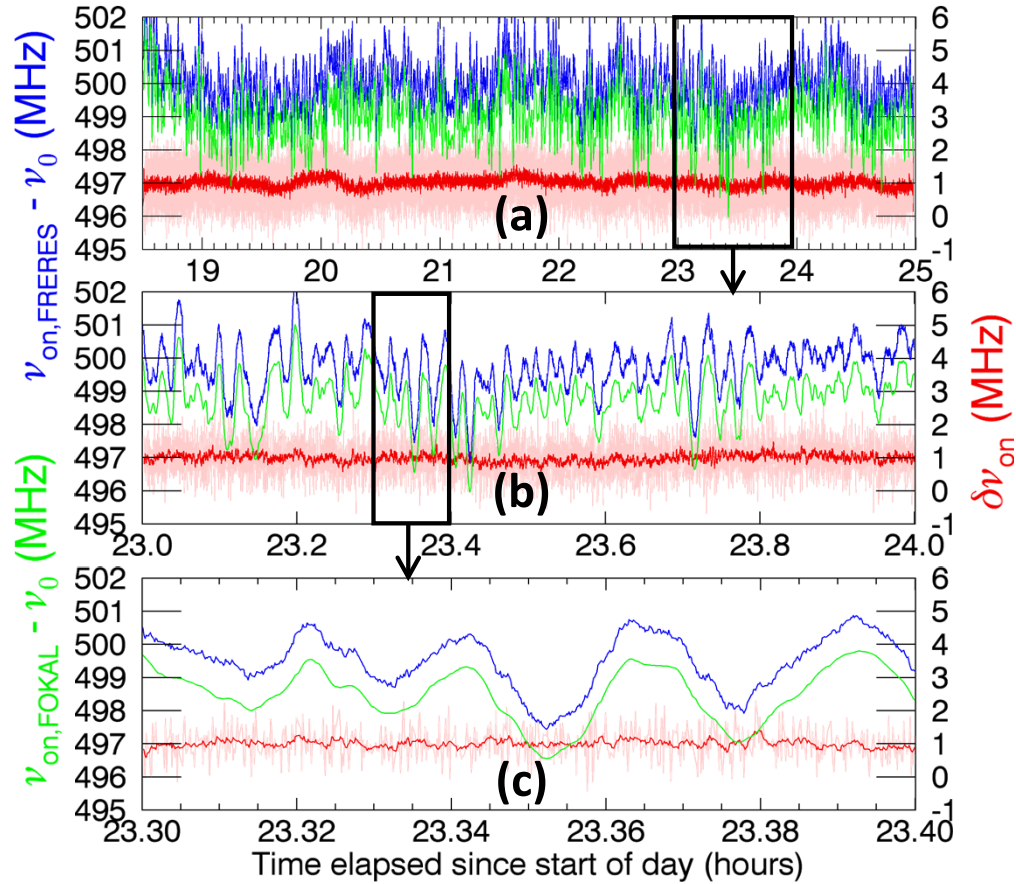


Fig. 3. (a) Full time series of $\nu_{on,FRERES} - \nu_0$ (blue, y-scale on the left), $\nu_{on,FOKAL} - \nu_0$ (green, y-scale on the left) and their difference $\delta\nu_{on}$ (red, y-scale on the right) as acquired during the return transfer flight on 16.09.2022 and calculated from FRERES and FOKAL data, with a 5 s gliding average applied, except for the light red curve which shows the data at the native time resolution of 2 Hz. For better readability of the y-scale, the frequencies are relative to ν_0 . (b) Subset of one hour within (a), time window indicated by a black rectangle. (c) Subset of 6 minutes within (b), time window indicated by a black rectangle.

However, the residual difference between the two measurements, $\delta\nu_{on}$, also plotted in Fig. 3, does show some short-term discrepancies and slowly varying biases. Furthermore, a systematic offset of the order of 1 MHz is visible. This affects all flights as illustrated in Fig. 4, which provides an overview of all available $\delta\nu_{on}$ time series in the dataset.

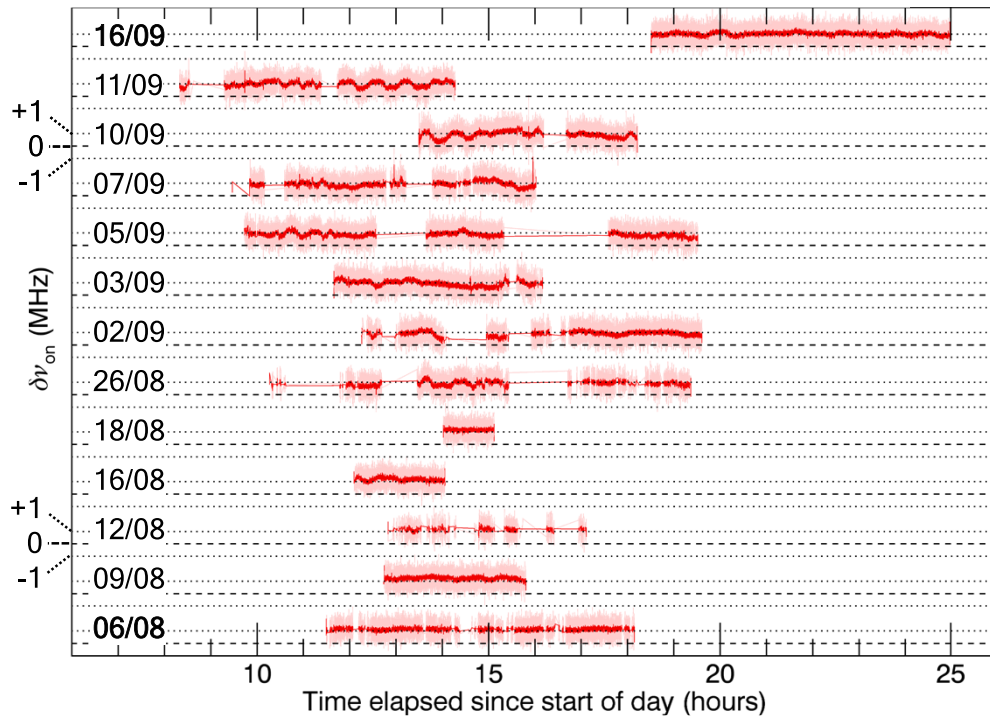


Fig. 4. Overview of the available $\delta\nu_{on}$ time series after comprehensive FOKAL data filtering and processing, at the native 2 Hz resolution (light red) and with a 5 s gliding average applied (red). The dashed lines indicate the $y = 0$ axis, the dotted lines the $y = +1$ MHz and $y = -1$ MHz axis for each flight. The date of each flight in 2022 is also indicated (transfer flights in bold).

5. Data analysis

5.1. Long-term stability of FRERES over several weeks

According to the absolute calibrations before and after the campaign with the stationary SRFC, the in-built CSAC RF reference in FOKAL provides sufficient long-term stability to investigate the long-term stability of FRERES over the six weeks of the whole CoMet 2.0 Arctic campaign, at least down to an accuracy of a few tens of kHz (cf section 2.2). For this we simply computed the mean value of $\delta\nu_{on}$ for each flight, and the results are shown in Fig. 5, with a dashed line pointing to the mid-campaign switch to a different modulation amplitude for the reference laser. The corresponding jump in the offset of the online seeder frequency can be explained by the slight non-linearity in the DFB laser diode's transfer function from current to optical frequency, which produces an amplitude-dependent asymmetry in the modulation waveform and corresponding amplitude-dependent shift in the position of the zero-crossing with respect to its theoretical position for sinusoidal modulation.

Regardless of this effect, which is reproducible and can be calibrated in the laboratory, there are hints of long-term drifts in the offset of FRERES with respect to FOKAL. Therefore, we fitted a linear model to each subset of data points, before and after the modulation amplitude change. In both cases, the fits point to a positive drift of the average position of the online seed laser over time, although the fitted slope is only statistically significant in the second half of the campaign. The calculated slope of about 0.1 to 0.2 MHz/month, extrapolated to the period of time between the FC1500 calibration of FRERES, at the end of May 2022, and the start of the campaign at the

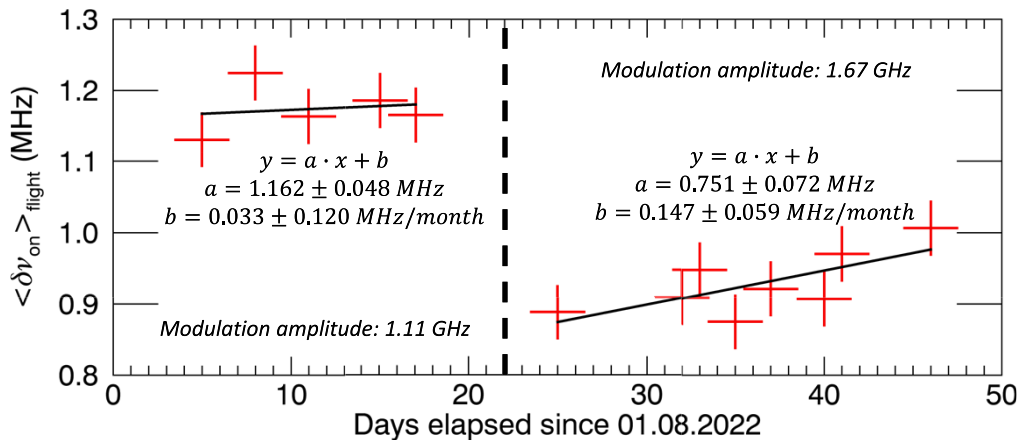


Fig. 5. Red crosses: mean value of $\delta\nu_{on}$ for each of the 13 time series from Fig. 4. A dashed line indicates the switch to a different modulation amplitude for the reference laser in FRERES in the second part of the campaign. Black lines: linear fits to the data before and after the modulation amplitude change.

beginning of August, could account for an offset of up to 0.4 ± 0.15 MHz (cf Table 2). However, this is still 0.55 MHz short of the observed offset of about 1.1 MHz at the beginning of August.

We hypothesize that these drifts are associated with a slow leak of ambient air into FRERES's absorption cell over time. Indeed, the air-induced pressure shifting coefficient for the CO_2 absorption line at $6361.2504 \text{ cm}^{-1}$ is negative, currently estimated to about $-0.0059 \text{ cm}^{-1} \cdot \text{atm}^{-1}$ according to the HITRAN 2020 database [18], which in turn still uses a value from [19]. This means that increasing air pressure in the cell shifts the line center, and thus the WMS zero-crossing, towards smaller optical frequencies. A frequency shift of -1 MHz would correspond to an increase of about 5 mbar of the pressure in the cell, equivalent to a leak rate of $3.3 \times 10^{-7} \text{ atm} \cdot \text{cm}^3 \cdot \text{s}^{-1}$ over two months when considering the 0.3-l volume of the cell. This is a plausible value compared to a specified leak rate of $10^{-8} \text{ atm} \cdot \text{cm}^3 \cdot \text{s}^{-1}$ for similarly designed gas flow cells with Viton O-rings [20].

Since it is not uncommon for leak rates in vacuum systems to be environmentally dependent and intermittent, we deem it likely that larger leaks of outside air into the absorption cell may have occurred during the transport of CHARM-F from the laboratory to the aircraft hangar for integration, and during the integration itself. This could account for the “missing” 0.55 MHz of offset between the laboratory calibration of FRERES and the start of the campaign when solely considering the observed drift rate in Canada.

5.2. In-flight stability of FRERES at timescales up to a few hours

The Allan deviation has established itself over the years as the tool of choice for the characterization of instabilities in oscillators, including lasers, but increasingly also for the classification and quantification of noise in a number of other fields including tunable diode laser spectroscopy and remote sensing [e.g. 21,22].

The power of the Allan deviation lies in its ability to quantify time-correlated noise over different correlation timescales. It is therefore only natural to introduce it into the context of IPDA column measurements of trace gases, where the greatest challenge lies in detecting weak concentration gradients over spatial scales ranging from a few tens to a few thousands of kilometers. For a spaceborne instrument flying at 7 km/s, this puts a requirement on correlated instrumental noise over a few tens of seconds to a few tens of minutes. For an airborne instrument

flying at 0.25 km/s such as CHARM-F, this puts a requirement on correlated noise over timescales of a few tens of seconds up to a few hours. Because of the position of the online wavelength in the wing of the absorption line (cf section 1), unknown instabilities of the emitted online wavelength directly translate into noise, therefore this is a critical contributor to the correlated noise budget.

Deriving a frequency stability/knowledge accuracy requirement, however, rests on the specific error budget allocation; a comprehensive ESA Phase 0 study for a spaceborne carbon dioxide lidar [1] puts the specification on the transmitter's online long-term optical frequency stability in the 20 kHz ("goal" requirement) to 100 kHz ("breakthrough" requirement) range when relying on the CO₂ absorption lines in the 1.6-micron region. In the frame of another ESA project related to frequency reference development for future spaceborne CO₂ IPDA lidars [23], we reformulated these requirements in terms of "Allan templates", whereby the specification is a function of averaging time, following a white noise slope of -1/2 at the shorter timescales while smoothly merging into a constant (effectively constraining 1/f noise) at the longer timescales.

We computed the Overlapping Allan Deviation (OADEV) of $\delta\nu_{on}$ independently for each flight using the Stable32 frequency stability analysis software [24]. The results are plotted in Fig. 6 along with the afore-mentioned Allan templates, and with the flights sorted into two groups: before and after the change in modulation amplitude of the FRERES reference laser. Also shown in Fig. 6 is the OADEV of a 3.5-hour FOKAL measurement carried out on ground during the CoMet 1.0 campaign in 2018 by locking the seed laser to the GPS-referenced FC-1500, essentially providing a measure of the stability of FOKAL referenced to its internal CSAC. We note that the FOKAL performance appeared in this case to be slightly worse than the performance quoted in the CSAC's datasheet and shown with a dash-dotted line in Fig. 6, but remains better than all $\delta\nu_{on}$ curves and better than the "goal" requirement by a comfortable margin up to the last data point allowed by the measurement duration, giving confidence in the assumption that the statistics of $\delta\nu_{on}$ are driven by FRERES and not by FOKAL in the CoMet 2.0 Arctic data.

As far as the flight data is concerned, a word of caution is in order for the interpretation of the OADEV, as almost all flights include a few gaps of varying length due to the intermittent issues with the FOKAL lock. Strictly speaking, the Allan deviation is only defined for continuous data, and some authors recommend to split intermittent data into smaller gapless blocks, or forgo the Allan analysis altogether for such data [24]. However, there is some literature on gap-filling strategies such as linear interpolation or more advanced techniques based on live data mirroring [25]. In practice, the strategy with intermittent data very much depends on the distribution of the gaps (length and frequency), the nature of the data and the goal of the analysis. For the present dataset, the argument can be made that gaps can be simply ignored, since the low frequency of occurrence of the gaps during each flight does not significantly alter the nature and amplitude of the noise in the measurement, but may only shift some features of the Allan curve towards shorter timescales.

This happens to be verifiable experimentally in the dataset itself, by qualitatively comparing the gap distribution per flight in Fig. 4 and the Allan curves of Fig. 6. Indeed, the 12/08 flight contains the most frequent and longest gaps relative to its duration, and the corresponding Allan curve, indicated with an arrow in Fig. 6, happens to be the only one whose "bump" peaks close to 100 s averaging time, while the others peak nearer to the 1000 s mark. These bumps, centered around to the 1000-s abscissa, can be attributed to the residual effect of étalon fringes within the absorption cell, which in turn correlate with temperature and pressure changes in the cabin, and appear as the limiting factor to the frequency stability of FRERES.

Another striking feature of Fig. 6 is the difference in the FRERES performance before and after the modulation amplitude change, with a factor 2 to 3 worse performance in the latter case. This is to some extent also visible in Fig. 4 in the form of larger "oscillations" on the residuals. We attribute this effect to the fact that the larger modulation amplitude does not fulfill condition (3) of section 3.1 as well as the smaller modulation amplitude, leading to a greater sensitivity of the

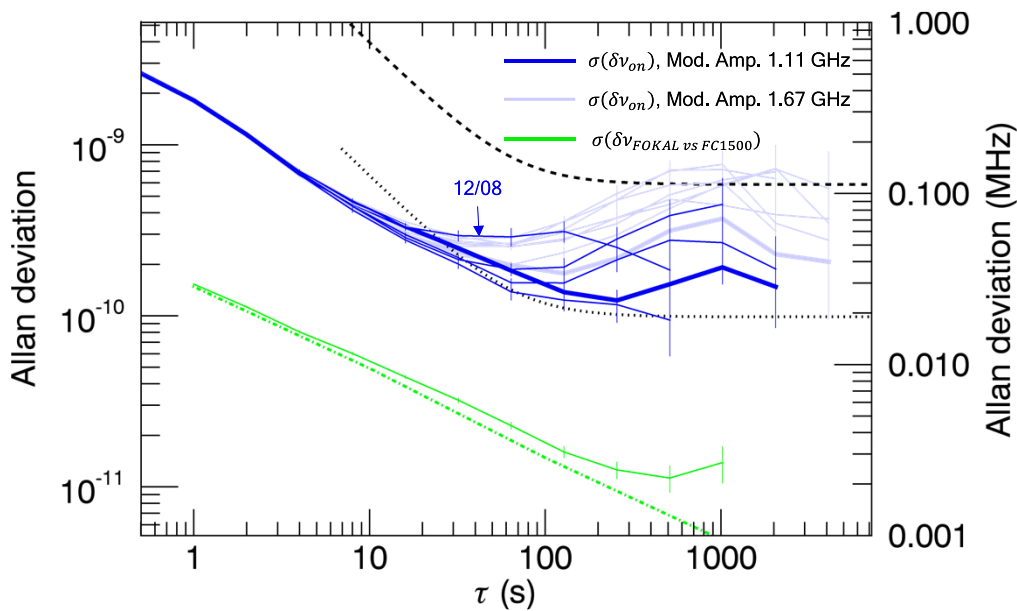


Fig. 6. Blue: OADEV of $\delta\nu_{on}$ as a function of averaging time τ for each of the 13 flights, sorted by modulation amplitude of the FRERES reference laser. The thick lines correspond to the transfer flights on 06/08/22 and 16/09/22. Black: “breakthrough” (dashed) and “goal” (dotted line) requirements for the online frequency stability of a spaceborne CO_2 IPDA lidar from [14]. Green, continuous: OADEV of the online seed laser locked to the stationary, GPS-referenced FC-1500 SRFC, as measured by FOKAL referenced to its internal CSAC. Green, dash-dotted: specified Allan deviation of the CSAC from [10]. All OADEV data points are plotted with the associated 1σ uncertainty computed with the Stable32 software following the method outlined in [24]. An additional vertical scale on the right-hand side shows the corresponding deviations in terms of optical frequency at 1572.02 nm.

system to étalon fringe movements correlated to the noisy thermal and mechanical environment in the aircraft. Within each subset of flights, we also note that the transfer flights, highlighted with thicker lines in Fig. 6, display the best performance with less pronounced bumps at longer averaging times: this is expected due to the more stable cabin environment during long flights at constant cruise altitude.

Finally, we can now comment quantitatively on the performance of FRERES under flight conditions. With the more optimal modulation amplitude, a frequency knowledge accuracy of better than 100 kHz over time intervals of several hours is reached by the system, putting it in-between the “threshold” and “goal” requirements for a spaceborne CO_2 IPDA lidar at 1.6 micron. This is less than a $1/5000^{\text{th}}$ of the width of the Doppler-broadened absorption line in the absorption cell, which is a remarkable achievement for a WMS-based system. For a position of the online channel in the wing of the line with the same offset as the baseline of the A-SCOPE phase 0 studies [1], this contributes to an uncertainty of only about 0.025% on the column-averaged carbon dioxide concentration. Nevertheless, using the more accurate information from the on-board SRFC allows an enhancement of the frequency accuracy by a factor of 10 at least, well below the “goal” requirement.

6. Conclusion

For the first time, to these authors' knowledge, a miniaturized, rugged SRFC was used to support airborne IPDA measurements of carbon dioxide during a large-scale flight campaign in 2022. It provided an independent assessment of the in-flight frequency stability of the CO₂ online channel of CHARM-F's WMS-based frequency reference subsystem, FRERES, over timescales ranging from a few hours up to a few months over the whole measurement campaign.

Thanks to the SRFC, the short-term stability of FRERES over a few hours within a measurement flight could be shown to be better than 0.1 MHz, equivalent to 1/5000th of the width of the Doppler-broadened CO₂ absorption line used as absolute reference in a multipass absorption cell and corresponding to an uncertainty of the order of only 0.025% on the column measurement. Long-term drifts of the same order of magnitude could also be detected and quantified over the campaign duration. This is a remarkable result for a WMS-based frequency stabilization scheme.

However, the SRFC measurements could be shown to enhance the frequency accuracy of the IPDA measurement by a factor of ten at least when using an off-the-shelf CSAC as RF reference, down to values well below the "goal" requirement for a spaceborne IPDA lidar for carbon dioxide operating in the 1.6-micron region. Furthermore, this accuracy can be reached at any wavelength within the broad spectral range accessible with SRFCs, provided suitable optical amplifiers and BDUs are used, making SRFCs a promising universal frequency reference for future airborne or spaceborne atmospheric lidars.

Funding. State of Bremen, the Max Planck Society (MPG); Deutsche Forschungsgemeinschaft (DFG); DFG Priority Program (SPP 1294); Atmospheric and Earth System Research (BO 1731/1-1); Deutsches Zentrum für Luft- und Raumfahrt (DLR) (MABAK, GHGMON).

Disclosures. The authors declare no conflicts of interest.

Data availability. Data underlying the results presented in this paper are not publicly available at this time but may be obtained from the authors upon reasonable request.

References

1. P. Ingmann, P. Bensi, Y. Durand, *et al.*, "Advanced Space Carbon and Climate Observation of Planet Earth, Report for Assessment," SP-1313/1, European Space Research and Technology Centre, European Space Agency, Noordwijk, The Netherlands (2009), https://esamultimedia.esa.int/docs/SP1313-1_ASCOPE.pdf.
2. G. Ehret, C. Kiemle, and M. Wirth, "Space-borne remote sensing of CO₂, CH₄, and N₂O by integrated path differential absorption lidar: a sensitivity analysis," *Appl. Phys. B* **90**(3-4), 593–608 (2008).
3. A. Fix, A. Amediek, H.-C. Büdenbender, *et al.*, "CH₄ and CO₂ IPDA Lidar measurements during the COMET 2018 airborne field campaign", *29th International Laser Radar Conference* (2019).
4. P. Zou, B. Sprenger, B. Pröbster, *et al.*, "Airborne frequency comb for greenhouse gas monitoring," *29th International Laser Radar Conference* (2019).
5. R. Holzwarth, Th. Udem, T. W. Hänsch, *et al.*, "Optical Frequency Synthesizer for Precision Spectroscopy," *Phys. Rev. Lett.* **85**(11), 2264–2267 (2000).
6. T. Udem, R. Holzwarth, and T. Hänsch, "Optical frequency metrology," *Nature* **416**(6877), 233–237 (2002).
7. W. Hänsel, H. Hoogland, M. Giunta, *et al.*, "All polarization-maintaining fiber laser architecture for robust femtosecond pulse generation," *Appl. Phys. B* **123**(1), 41 (2017).
8. U.S. patent 8873601B2 (28 Oct. 2014).
9. M. Lezius, T. Wilken, C. Deutsch, *et al.*, "Space-borne frequency comb metrology," *Optica* **3**(12), 1381–1387 (2016).
10. Symmetricom (now Microchip) DS/SA.45s datasheet, CSAC/081611.
11. M. Quatrevalet, A. Amediek, A. Fix, *et al.*, "CHARM-F: The Airborne Integral Path Differential Absorption Lidar for Simultaneous Measurements of Atmospheric CO₂ and CH₄," *25th International Laser Radar Conference* (2010).
12. A. Amediek, G. Ehret, A. Fix, *et al.*, "CHARM-F - a new airborne integrated-path differential-absorption lidar for carbon dioxide and methane observations: measurement performance and quantification of strong point source emissions," *Appl. Opt.* **56**(18), 5182–5197 (2017).
13. P. Mahnke, M. Wirth, and A. Fix, "OPO resonator length stabilisation for injection seeding using fibre coupled heterodyne detection," *Conference on Lasers and Electro-Optics/Quantum Electronics and Laser Science Conference and Photonic Applications Systems Technologies*, paper JWA23 (2008).
14. M. Wirth, A. Fix, P. Mahnke, *et al.*, "The airborne multi-wavelength water vapor differential absorption lidar WALES: system design and performance," *Appl. Phys. B* **96**(1), 201–213 (2009).
15. J. B. McManus and P. L. Kebabian, "Narrow optical interference fringes for certain setup conditions in multipass absorption cells of the Herriott type," *Appl. Opt.* **29**(7), 898–900 (1990).

16. J. B. McManus, M. S. Zahniser, and D. D. Nelson, "Dual quantum cascade laser trace gas instrument with astigmatic Herriott cell at high pass number," *Appl. Opt.* **50**(4), A74–A85 (2011).
17. R. Koga, M. Kosaka, and H. Sano, "Improvement of Etalon-fringe Immunity in Diode-laser Derivative Spectroscopy," *Memoirs of the School of Engineering, Okayama University* **16**(1), 1 (1981).
18. I.E. Gordon, L. S. Rothman, R. J. Hargreaves, *et al.*, "The HITRAN2020 molecular spectroscopic database," *J. Quant. Spectrosc. Radiat. Transfer* **277**, 107949 (2022).
19. J.-M. Hartmann, "A simple empirical model for the collisional spectral shift of air-broadened CO₂ lines," *J. Quant. Spectrosc. Radiat. Transfer* **110**(18), 2019–2026 (2009).
20. <https://www.wavelengthreferences.com/wp-content/uploads/Data-FCW-2019.pdf>.
21. P. Werle, R. Mücke, and F. Slemr, "The limits of signal averaging in atmospheric trace-gas monitoring by tunable diode-laser absorption spectroscopy (TDLAS)," *Appl. Phys. B* **57**(2), 131–139 (1993).
22. D. V. Land, A. P. Levick, and J. W. Hand, "The use of the Allan deviation for the measurement of the noise and drift performance of microwave radiometers," *Meas. Sci. Technol.* **18**(7), 1917–1928 (2007).
23. A. Fix, R. Matthey, A. Amediek, *et al.*, "Investigations on frequency and energy references for a space-borne integrated path differential absorption lidar," *Proc. SPIE* **10563**, 105630A (2017).
24. W. Riley and D. Howe, "Handbook of Frequency Stability Analysis," *Special Publication 1065*, National Institute of Standards and Technology, https://tsapps.nist.gov/publication/get_pdf.cfm?pub_id=50505.
25. D. A. Howe and N. Schlossberger, "Characterizing Frequency Stability Measurements Having Multiple Data Gaps," *IEEE Trans. Ultrason., Ferroelect., Freq. Contr.* **69**(2), 468–472 (2022).